Exact solutions for free vibration analysis of laminated, box and sandwich beams by refined layer-wise theory

Exact solutions for free vibration analysis of laminated, box and sandwich beams by refined layer-wise theory

Yan Yang[a,b*], Alfonso Pagani[b†], Erasmo Carrera[b‡]

[a] *College of Mechanics and Materials, Hohai University, 210098, Nanjing, China*

[b] *MuI², Department of Mechanical and Aerospace Engineering, Politecnico di Torino, Corso Duca degli Abruzzi 24, 10129 Torino, Italy.*

Submitted to

Composite Structures

Author for correspondence:
E. Carrera, Professor of Aerospace Structures and Aeroelasticity,
Department of Mechanical and Aerospace Engineering,
Politecnico di Torino,
Corso Duca degli Abruzzi 24,
10129 Torino, Italy,
tel: +39 011 090 6836,
fax: +39 011 090 6899,
e-mail: erasmo.carrera@polito.it

*PhD Student, e-mail: yanyanghhu@hhu.edu.cn
†Assistant Professor, e-mail: alfonso.pagani@polito.it
‡Professor of Aerospace Structures and Aeroelasticity, e-mail: erasmo.carrera@polito.it

ABSTRACT

The present work addresses a closed-form solution for the free vibration analysis of simply supported composite laminated beams via a refined one-dimensional (1D) model, which employs the Carrera Unified Formulation (CUF). In the framework of CUF, the 3D displacement field can be expanded as any order of generic unknown variables over the cross section , in the case of beam theories. Particularly, Lagrange expansions of cross-sectional displacement variables in conjunction with layer-wise (LW) theory are adopted in this analysis, which makes it possible to refine the kinematic fields of complex cross section by arbitrary order and accuracy. As a consequence, the governing equations can be derived using the principle of virtual work in a unified form and can be solved by a Navier-type, closed-form solution. Numerical investigations are carried out to test the performance of this novel method, including composite and sandwich beams ranging from simple to complex configurations of the cross section. The results are compared with those available in the literature as well as the 3D finite element method (FEM) solutions computed by commercial codes. The present CUF model is proved to be able of achieving high accurate results with less computational costs. Besides, they may serve as benchmarks for future assessments in this field.

Keywords: Carrera unified formulation; Layer-wise approach; Closed-form solution; Free vibration analysis

1 Introduction

Composite beams, as basic structural components, have been widely used in various engineering fields such as aerospace, mechanical, civil and ocean engineering due to their high strength- and stiffness-to-weight ratios. Also, determination of vibration characteristics is of crucial importance in the safe design of composite beams subjected to dynamic loads. Compared with the isotropic homogeneous elastic beam [1], composite structures present more complex material properties (anisotropy as well as fiber angle, and laminate stacking sequence), resulting in non classical vibration modes phenomena with couplings between torsion, shear and bending. These effects cannot be detected by 1D lower-order models, which were firstly extrapolated from classical theories under the assumptions outlined by Euler-Bernoulli [2]. As a result, it becomes essential to develop a simple yet accurate composite beam model to describe these specific mechanical behaviours correctly.

Refined 1D beam models have received widespread attention owing to their simplicity and higher-efficient computing performance. Over the years, several 1D refined composite beam models have been systematically developed for different engineering purposes. As far as the free vibration analysis is concerned, a brief overview of recent research on these refined 1D models is reported here. The first-order shear deformation theory (FSDT), as the improvement of Euler-Bernoulli beam theory, was proposed as an extension of the plate theories of Reissner [3] and Mindlin [4], which assume a constant transverse shear deformation in the thickness direction. Nevertheless, this assumption does not conform to stress-free boundary conditions. Thus, a shear correction factor was introduced to correct this theory and contributed to fruitful results [5, 6]. Since accurate estimation of the shear correction factor exerts much effort, several high-order shear deformation theories (HSDT) were proposed, which provided different distributions of the transverse shear strains along the thickness. In details, Khedeir and Reddy [7], employed a parabolic form of HSDT to study the free vibration behaviour of cross-ply laminated beams with arbitrary boundary conditions via a Navier-type analytical solution. Arya et al. [8] presented a trigonometric HSDT for the static analysis of symmetric cross-ply laminated beam, and Li et al. [9] extended this refined model to study free vibration of angle-ply laminated beam with general boundary conditions. Vidal and Polit [10] introduced a three-node beam element to perform the free vibration of composite and sandwich beams based on the trigonometric HSDT. A exponential HSDT was used for the bending, buckling and free vibration analyses of multi-layered laminated composite beams by Karama et al. [11], showing that the proposed model was more precise than the trigonometric HSDT model and FEM model studied early by Karama et al. [12]. In addition, other HSDT models [13] have been developed by various authors for describing the deformation through the thickness.

It should be noted that the above models were implemented on the basis of an Equivalent Single Layer (ESL) approach, which hypothesizes a continuous and differentiable displacement function through the thickness direction. Unfortunately, this assumption cannot account for the continuity of the transverse stresses and the zig-zag behavior of the displacements along the thickness. Therefore, a more precise hypothesis called layer-wise theory was put forward to overcome this drawback. In the domain of LW, a continuous displace-

ment function is adopted for each layer, and, as a consequence, a discontinuous derivative of displacement function is imposed at the intra-layer interfaces, thereby, meeting the fundamental requirements demanded by modelling of laminated structures. Shimpi and Ainapure [14] used LW theory to study the natural frequencies of simply supported two-layer beam in combination with the trigonometric HSDT. Tahani [15] investigated the static and dynamic properties of composite beam with general laminations using two different strategies based on LW theory. Plagianakos and Saravanos [16] applied the finite element method to predict damping and natural frequencies of thick composite and sandwich beams via a parabolic HSDT in conjunction with LW theory.

In contrast to ESL theory, burdensome computation cost may be required in LW theory, being dependent on the number of laminate layers. Therefore, several layer-independent theories have been developed on the premise of additional computational capacity and consumed time. In these theories, zig-zag or Heaviside functions were added in the framework of ESL theory. Carrera [17] presented a thorough review of Murakami's zig-zag method [18], who added a zig-zag function to approximate the thickness distribution of in-plane displacements. Furthermore, Carrera et al. [19] extended this theory to the static analysis of symmetric and antisymmetric cross-ply laminated beams, based on polynomial, trigonometric, exponential HSDT, respectively. Filippi and Carrera [20] made use of a higher-order zig-zag function to predict the natural frequencies of laminated and sandwich beams with lower slenderness ratio values. Other classes of Heaviside functions can be found in [21, 22].

Although the above refined theories can improve the accuracy of results significantly, it is a matter of fact that many of them are problem-dependent. Motivated by this deficiency, it is of notable importance to introduce a unified formulation which can be suitable for any structural composite beam. Carrera et al. [23] proposed this unified formulation, which was later denoted to as Carrera Unified Formulation (CUF). CUF was originally considered for the analysis of plate and shell structures, hereafter referred to as 2D CUF [24, 25, 26] and continued to be employed for beam structures, hereafter referred to as 1D CUF [27, 28]. In the light of 1D CUF, the 3D displacement field can be expanded elegantly as any order of the generalized unknown variables over the cross section. Moreover, the order of expansions can be regarded as a free parameter depending on the problem under consideration. In addition, FSDT and HSDT can be effortlessly derived in a hierarchical and compact way in the domain of CUF. Carrera et al. [29] used Taylor series polynomials as displacement expansions to obtain 3D stress states of beams with arbitrary cross-sectional geometries via 1D CUF FEM. The corresponding model is called 1D CUF Taylor expansion (TE), which has been likewise applied to the free vibration analysis [30, 31, 32], buckling phenomenon [33], composite beams [34, 35, 36] and functional graded beams [37, 38]. Recently, a new class of CUF model was proposed by Carrera and Petrolo. [39], where displacements are approximated by the sum of cross-sectional node displacement unknowns via Lagrange expansion (LE), being inhere LW ability. This 1D CUF LE model permits one to analyze behaviours of beams with more complex geometry shape with less computational costs. Carrera et al. [40] adopted TE and LE

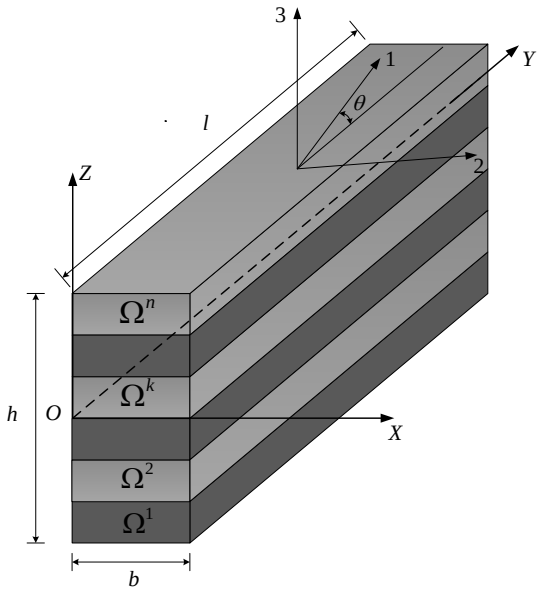

Figure 1: Physical coordinate system for a laminated composite beam.

CUF for the in-plane and out-of-plane stress analysis of compact and multi-cell laminated box beams by using FEM, in which, TE is implemented along with ESL, whereas, LW is carried out in the framework of LE. Then, the same authors extended static analysis to the free vibration problem, readily detecting solid and shell-like phenomena [41]. Other important CUF model are those on the basis of Chebyshev Expansions (CE) [42] and Hierarchical Legendre-type Expansions (HLE) [43].

In contrast to the 1D CUF model solved by weak-form solution, e.g., FEM, Giunta et al. provided a strong-form solution, namely, Navier-type solution of the 1D CUF TE governing equation for the free vibration analysis of composite beam [37] and staic, buckling and free vibration analysis of sandwich beams [44, 45]. The extension of the Navier-type closed-form solution to the 1D CUF LE for free vibration analysis of isotropic beams was done by Dan et al. [46].

In the present paper, for the first time, the same analytical solution is utilized for the free vibration of cross-ply composite beam with compact and thin-walled cross sections subject to the simply supported boundary conditions based on 1D CUF LE model and LW theory. The rest of this paper is structured as follows: (i) a brief introduction of anisotropic elasticity theory and 1D CUF LE theory are given in Section 2.1; (ii) The equations of motion and corresponding boundary conditions are derived using principle of virtual work in Section 2.2 and a linear eigensystem is obtained using the Navier-type closed-form solution in Section 2.3; (iii) The numerical results of different assessments considered are presented in Section 3; (iv) some conclusions and remarks of this work are outlined in the last section.

2 1D CUF beam theory

2.1 Preliminaries

Consider a multi-layer laminated beam in physical coordinate system, as shown in Fig.1. Assume that y-axis is coincident with the longitudinal axis of the beam and its cross section is defined on the xz-plane, being denoted as Ω. The superscript k stands for the number of the generic layer, starting from the bottom to top. The three-dimensional displacement vector for kth layer is introduced as follows:

$$\mathbf{u}^k(x,y,z;t) = \left\{u_x^k \; u_y^k \; u_z^k\right\}^{\mathrm{T}} \tag{1}$$

where u_x^k, u_y^k and u_z^k indicate the displacement components along three axes x, y, z, respectively. The index "T" denotes the transpose operator. Similarly, stress $\boldsymbol{\sigma}$ and strain $\boldsymbol{\epsilon}$ components can be arranged as:

$$\boldsymbol{\sigma}^k = \left\{\sigma_{yy}^k \; \sigma_{xx}^k \; \sigma_{zz}^k \; \sigma_{xz}^k \; \sigma_{yz}^k \; \sigma_{xy}^k\right\}^{\mathrm{T}}, \quad \boldsymbol{\epsilon}^k = \left\{\epsilon_{yy}^k \; \epsilon_{xx}^k \; \epsilon_{zz}^k \; \epsilon_{xz}^k \; \epsilon_{yz}^k \; \epsilon_{xy}^k\right\}^{\mathrm{T}} \tag{2}$$

Based on the assumption of small displacements and strains, the relationship between ($\boldsymbol{\sigma}$) and ($\boldsymbol{\epsilon}$) can be expressed as:

$$\boldsymbol{\epsilon}^k = \mathbf{D}\mathbf{u}^k \tag{3}$$

where

$$\mathbf{D} = \begin{bmatrix} 0 & \dfrac{\partial}{\partial y} & 0 \\ \dfrac{\partial}{\partial x} & 0 & 0 \\ 0 & 0 & \dfrac{\partial}{\partial z} \\ \dfrac{\partial}{\partial z} & 0 & \dfrac{\partial}{\partial x} \\ 0 & \dfrac{\partial}{\partial z} & \dfrac{\partial}{\partial y} \\ \dfrac{\partial}{\partial y} & \dfrac{\partial}{\partial x} & 0 \end{bmatrix} \tag{4}$$

In the case of laminated composite materials, the constitutive equation for kth layer assumes the following form:

$$\boldsymbol{\sigma}^k = \tilde{\mathbf{C}}^k \boldsymbol{\epsilon}^k \tag{5}$$

where

$$\tilde{\mathbf{C}}^k = \begin{bmatrix} \tilde{C}^k_{11} & \tilde{C}^k_{12} & \tilde{C}^k_{13} & 0 & 0 & \tilde{C}^k_{36} \\ \tilde{C}^k_{21} & \tilde{C}^k_{22} & \tilde{C}^k_{23} & 0 & 0 & \tilde{C}^k_{26} \\ \tilde{C}^k_{31} & \tilde{C}^k_{32} & \tilde{C}^k_{33} & 0 & 0 & \tilde{C}^k_{16} \\ 0 & 0 & 0 & \tilde{C}^k_{44} & \tilde{C}^k_{45} & 0 \\ 0 & 0 & 0 & \tilde{C}^k_{45} & \tilde{C}^k_{55} & 0 \\ \tilde{C}^k_{16} & \tilde{C}^k_{26} & \tilde{C}^k_{36} & 0 & 0 & \tilde{C}^k_{66} \end{bmatrix} \tag{6}$$

Coefficients in the matrix above are function of three parameters: Young modulus, Poisson ratios and fiber orientation angle (θ) measured down from the positive y-axis. For the sake of brevity and clarity, we do not provide the detailed expressions, one can refer to Reddy [47] for further details.

The generic displacement field, within the framework of CUF, can be expanded as arbitrary functions F_τ:

$$\mathbf{u}^k(x, y, z; t) = F_\tau(x, z)\mathbf{u}^k_\tau(y; t) \qquad \tau = 1, 2, ..., M \tag{7}$$

where F_τ is a function depending on the x and z coordinates. $\mathbf{u}_\tau$ is the generic displacements vector of axial coordinates y. M is the number of expanded terms, and the repeated subscript, τ, stands for summation.

In this study, Lagrange expansion polynomials are employed as the function F_τ to discrete the arbitrarily complex cross section, whose approximation precision lies on the order of LE polynomials. Three types of LE polynomials, i.e., four-node quadrilateral L4, nine-node cubic L9, and sixteen-node quartic L16 polynomials, are often adopted. The expression of L9 polynomial is presented here as an illustrative example:

$$\begin{aligned} F_\tau &= \tfrac{1}{4}(\mathrm{r}^2 + \mathrm{r}\ \mathrm{r}_\tau)(\mathrm{s}^2 + \mathrm{s}\ \mathrm{s}_\tau) \qquad \tau = 1, 3, 5, 7 \\ F_\tau &= \tfrac{1}{2}\mathrm{s}^2_\tau(\mathrm{s}^2 - \mathrm{s}\ \mathrm{s}_\tau)(1 - r^2) + \tfrac{1}{2}\mathrm{r}^2_\tau(\mathrm{r}^2 - \mathrm{r}\ \mathrm{r}_\tau)(1 - \mathrm{s}^2) \qquad \tau = 2, 4, 6, 8 \\ F_\tau &= (1 - \mathrm{r}^2)(1 - \mathrm{s}^2) \qquad \tau = 9 \end{aligned} \tag{8}$$

where r and s vary over the interval $[-1,\ +1]$, and r_τ and s_τ indicate the vertex location in the natural coordinate system. For more details about the other two kinds of LE polynomials, see Carrera and Petrolo [39].

The nine-node cubic single-L9 kinematic field is therefore given by:

$$\begin{aligned} u^k_x &= F_1 u^k_{x_1} + F_2 u^k_{x_2} + F_3 u^k_{x_3} + F_4 u^k_{x_4} + F_5 u^k_{x_5} + F_6 u^k_{x_6} + F_7 u^k_{x_7} + F_8 u^k_{x_8} + F_9 u^k_{x_9} \\ u^k_y &= F_1 u^k_{y_1} + F_2 u^k_{y_2} + F_3 u^k_{y_3} + F_4 u^k_{y_4} + F_5 u^k_{y_5} + F_6 u^k_{y_6} + F_7 u^k_{y_7} + F_8 u^k_{y_8} + F_9 u^k_{y_9} \\ u^k_z &= F_1 u^k_{z_1} + F_2 u^k_{z_2} + F_3 u^k_{z_3} + F_4 u^k_{z_4} + F_5 u^k_{z_5} + F_6 u^k_{z_6} + F_7 u^k_{z_7} + F_8 u^k_{z_8} + F_9 u^k_{z_9} \end{aligned} \tag{9}$$

where $u^k_{x_1}, ..., u^k_{z_9}$ are the nine-node translational displacement variables of the problem considered.

The present LE model can be refined either with higher-order polynomials (global refinement) or a combination of polynomials in each sub-domain cross section (local refinement). For the sake of brevity, the following derivations are carried out on the kth layer and superscript k will be omitted.

2.2 Equations of motion

Equations of motion and corresponding boundary conditions can be obtained via the variational principle of virtual work.

$$\delta L = \delta L_{\text{int}} + \delta L_{\text{ine}} = 0 \tag{10}$$

where δ is the symbol of a virtual variation. L_{int} stands for the strain energy, L_{ine} represents the inertial work.

The strain energy can be expressed as follows:

$$\delta L_{\text{int}} = \int_V \delta \boldsymbol{\epsilon}^{\mathrm{T}} \boldsymbol{\sigma} \mathrm{d}V \tag{11}$$

Substituting Eq. (3), Eq. (5) and Eq. (7) into Eq. (11) and using the integration by parts (see [48]), one has:

$$\delta L_{\text{int}} = \int_l (\delta \boldsymbol{u}_\tau)^{\mathrm{T}} \mathbf{K}^{\tau s} \boldsymbol{u}_s \mathrm{d}y + \left[(\delta \boldsymbol{u}_\tau)^{\mathrm{T}} \boldsymbol{\Pi}^{\tau s} \boldsymbol{u}_s\right] |_{y=0}^{y=l} \tag{12}$$

where $\mathbf{K}^{\tau s}$ is fundamental nucleus of the stiffness, $\boldsymbol{\Pi}^{\tau s}$ represents the mechanical boundary conditions and l is the length of the beam. They are both 3×3 matrices. For the sake of brevity, the explicit expressions concerning these fundamental nuclei are not reported here, but are available from the corresponding literature [36]. It is envisaged that the term $\left[(\delta \boldsymbol{u}_\tau)^{\mathrm{T}} \boldsymbol{\Pi}^{\tau s} \boldsymbol{u}_s\right] |_{y=0}^{y=l}$ is equal to zero in the case of simply supported beam and will be removed in the following equations.

The virtual variation of the inertial work is defined as:

$$\delta L_{\text{ine}} = \int_V \rho \delta \boldsymbol{u} \ddot{\boldsymbol{u}} \mathrm{d}V \tag{13}$$

where ρ stands for the density of material and and the superimposed dots denote double derivative with respect to time (t). Accounting for Eq. (7), Eq. (13) can be rewritten as:

$$\delta L_{\text{ine}} = \int_l \delta \boldsymbol{u}_\tau \mathbf{M}^{\tau s} \ddot{\boldsymbol{u}}_s \mathrm{d}y \tag{14}$$

The components of the 3×3 mass matrix $\mathbf{M}^{\tau s}$ are:

$$M_{ij}^{\tau s} = \delta_{ij} E_{\tau s}^{\rho} \qquad i, j = 1, \cdots, 3 \tag{15}$$

where δ_{ij} is the Dirac's delta function and:

$$E^{\rho}_{\tau s} = \int_{\Omega} \rho F_{\tau} F_{s} \mathrm{d}\Omega \tag{16}$$

The explicit expression of the dynamic governing equations can be obtained from the principle of virtual displacements as follows:

$$\begin{aligned}
\delta u_{x\tau}: \quad & -E^{66}_{\tau s} u_{xs,yy} + \big(E^{26}_{\tau,x s} - E^{26}_{\tau s,x}\big) u_{xs,y} + \big(E^{22}_{\tau,x s,x} + E^{44}_{\tau,z s,z}\big) u_{xs} \\
& -E^{36}_{\tau s} u_{ys,yy} + \big(E^{23}_{\tau,x s} - E^{66}_{\tau s,x}\big) u_{ys,y} + \big(E^{26}_{\tau,x s,x} + E^{45}_{\tau,z s,z}\big) u_{ys} \\
& +\big(E^{45}_{\tau,z s} - E^{16}_{\tau s,z}\big) u_{zs,y} + \big(E^{44}_{\tau,z s,x} + E^{12}_{\tau,x s,z}\big) u_{zs} = -E^{\rho}_{\tau s} \ddot{u}_{xs} \\
\delta u_{y\tau}: \quad & -E^{36}_{\tau s} u_{xs,yy} + \big(E^{66}_{\tau,x s} - E^{23}_{\tau s,x}\big) u_{xs,y} + \big(E^{26}_{\tau,x s,x} + E^{45}_{\tau,z s,z}\big) u_{xs} \\
& -E^{33}_{\tau s} u_{ys,yy} + \big(E^{36}_{\tau,x s} - E^{36}_{\tau s,x}\big) u_{ys,y} + \big(E^{66}_{\tau,x s,x} + E^{55}_{\tau,z s,z}\big) u_{ys} \\
& +\big(E^{55}_{\tau,z s} - E^{13}_{\tau s,z}\big) u_{zs,y} + \big(E^{16}_{\tau,x s,z} + E^{45}_{\tau,z s,x}\big) u_{zs} = -E^{\rho}_{\tau s} \ddot{u}_{ys} \\
\delta u_{z\tau}: \quad & \big(E^{16}_{\tau,z s} - E^{45}_{\tau s,z}\big) u_{xs,y} + \big(E^{44}_{\tau,x s,z} + E^{12}_{\tau,z s,x}\big) u_{xs} \\
& +\big(E^{13}_{\tau,z s} - E^{55}_{\tau s,z}\big) u_{ys,y} + \big(E^{45}_{\tau,x s,z} + E^{16}_{\tau,z s,x}\big) u_{ys} - E^{55}_{\tau s} u_{zs,yy} \\
& +\big(E^{45}_{\tau,x s} - E^{45}_{\tau s,x}\big) u_{zs,y} + \big(E^{44}_{\tau,x s,x} + E^{11}_{\tau,z s,z}\big) u_{zs} = -E^{\rho}_{\tau s} \ddot{u}_{zs}
\end{aligned} \tag{17}$$

where the suffix after the comma indicates the derivatives and the generic term $E^{\alpha\beta}_{\tau,\theta s,\zeta}$ is a cross-sectional moment parameter:

$$E^{\alpha\beta}_{\tau,\theta s,\zeta} = \int_{\Omega} \tilde{C}_{\alpha\beta} F_{\tau,\theta} F_{s,\zeta} \mathrm{d}\Omega \tag{18}$$

2.3 Analytical solution

In the case of simply supported composite beam, the analytical solution of the above differential equations can be obtained via a Navier-type solution. The displacement fields are assumed as a sum of harmonic functions:

$$\begin{aligned}
u_{xs}(y;t) &= U_{xs} \sin(\alpha y) e^{i\omega t} \\
u_{ys}(y;t) &= U_{ys} \cos(\alpha y) e^{i\omega t}
\end{aligned} \tag{19}$$

$$u_{zs}(y;t) = U_{zs}\sin(\alpha y)e^{i\omega t}$$

where α is:

$$\alpha = \frac{m\pi}{l} \tag{20}$$

where U_{xs}, U_{ys} and U_{zs} are the amplitudes of the components of the generalized displacements vector. m is the half wave number along the beam axis, ω is the vibrational natural frequency and i is the imaginary unit. Substituting Eq. (19) into Eq. (17), it holds:

$$\begin{aligned}
\delta U_{x\tau}: \quad & \alpha^2 E^{66}_{\tau s} U_{xs}\sin(\alpha y) + \alpha\big(E^{26}_{\tau,_x s} - E^{26}_{\tau s,_x}\big)U_{xs}\cos(\alpha y) + \big(E^{22}_{\tau,_x s,_x} + E^{44}_{\tau,_z s,_z}\big)U_{xs}\sin(\alpha y) \\
& + \alpha^2 E^{36}_{\tau s} U_{ys}\cos(\alpha y) - \alpha\big(E^{23}_{\tau,_x s} - E^{66}_{\tau s,_x}\big)U_{ys}\sin(\alpha y) + \big(E^{26}_{\tau,_x s,_x} + E^{45}_{\tau,_z s,_z}\big)U_{ys}\cos(\alpha y) \\
& + \alpha\big(E^{45}_{\tau,_z s} - E^{16}_{\tau s,_z}\big)U_{zs}\cos(\alpha y) + \big(E^{44}_{\tau,_z s,_x} + E^{12}_{\tau,_x s,_z}\big)U_{zs}\sin(\alpha y) = \omega^2 E^{\rho}_{\tau s} U_{xs}\sin(\alpha y) \\
\delta U_{y\tau}: \quad & \alpha^2 E^{36}_{\tau s} U_{xs}\sin(\alpha y) + \alpha\big(E^{66}_{\tau,_x s} - E^{23}_{\tau s,_x}\big)U_{xs}\cos(\alpha y) + \big(E^{26}_{\tau,_x s,_x} + E^{45}_{\tau,_z s,_z}\big)U_{xs}\sin(\alpha y) \\
& + \alpha^2 E^{33}_{\tau s} U_{ys}\cos(\alpha y) - \alpha\big(E^{36}_{\tau,_x s} - E^{36}_{\tau s,_x}\big)U_{ys}\sin(\alpha y) + \big(E^{66}_{\tau,_x s,_x} + E^{55}_{\tau,_z s,_z}\big)U_{ys}\cos(\alpha y) \\
& + \alpha\big(E^{55}_{\tau,_z s} - E^{13}_{\tau s,_z}\big)U_{zs}\cos(\alpha y) + \big(E^{16}_{\tau,_x s,_z} + E^{45}_{\tau,_z s,_x}\big)U_{zs}\sin(\alpha y) = \omega^2 E^{\rho}_{\tau s} U_{ys}\cos(\alpha y) \\
\delta U_{z\tau}: \quad & \alpha\big(E^{16}_{\tau,_z s} - E^{45}_{\tau s,_z}\big)U_{xs}\cos(\alpha y) + \big(E^{44}_{\tau,_x s,_z} + E^{12}_{\tau,_z s,_x}\big)U_{xs}\sin(\alpha y) \\
& - \alpha\big(E^{13}_{\tau,_z s} - E^{55}_{\tau s,_z}\big)U_{ys}\sin(\alpha y) + \big(E^{45}_{\tau,_x s,_z} + E^{16}_{\tau,_z s,_x}\big)U_{ys}\cos(\alpha y) + \alpha^2 E^{55}_{\tau s} U_{zs}\sin(\alpha y) \\
& + \alpha\big(E^{45}_{\tau,_x s} - E^{45}_{\tau s,_x}\big)U_{zs}\cos(\alpha y) + \big(E^{44}_{\tau,_x s,_x} + E^{11}_{\tau,_z s,_z}\big)U_{zs}\sin(\alpha y) = \omega^2 E^{\rho}_{\tau s} U_{zs}\sin(\alpha y)
\end{aligned} \tag{21}$$

It is important to underline that the governing equation can be decoupled by setting the material parameters $\tilde{C}_{16}$,$\tilde{C}_{26}$, $\tilde{C}_{36}$, $\tilde{C}_{45}$ to be zero, which means isotropic or cross-ply laminate beams. Thus the above equations can be converted into the algebraic eigensystem as:

$$(\mathbf{K}^{\tau s} - \omega^2 \mathbf{M}^{\tau s})\boldsymbol{U} = 0 \tag{22}$$

where

$$
\begin{aligned}
&K_{xx}^{\tau s}=\alpha^2 E_{\tau s}^{66}+E_{\tau_{,x}s_{,x}}^{22}+E_{\tau_{,z}s_{,z}}^{44}, K_{xy}^{\tau s}=\alpha\left(E_{\tau_{,x}s}^{23}-E_{\tau s_{,x}}^{66}\right), K_{xz}^{\tau s}=E_{\tau_{,z}s_{,x}}^{44}+E_{\tau_{,x}s_{,z}}^{12}\\
&K_{yx}^{\tau s}=\alpha\left(E_{\tau_{,x}s}^{66}-E_{\tau s_{,x}}^{23}\right), K_{yy}^{\tau s}=\alpha^2 E_{\tau s}^{33}+E_{\tau_{,x}s_{,x}}^{66}+E_{\tau_{,z}s_{,z}}^{55}, K_{yz}^{\tau s}=\alpha\left(E_{\tau_{,z}s}^{55}-E_{\tau s_{,z}}^{13}\right)\\
&K_{zx}^{\tau s}=E_{\tau_{,x}s_{,z}}^{44}+E_{\tau_{,z}s_{,x}}^{12}, K_{zy}^{\tau s}=\alpha^2 E_{\tau s}^{55}+\alpha\left(E_{\tau_{,z}s}^{13}-E_{\tau s_{,z}}^{55}\right), K_{zz}^{\tau s}=E_{\tau_{,x}s_{,x}}^{44}+E_{\tau_{,z}s_{,z}}^{11}\\
&M_{xx}^{\tau s}=M_{yy}^{\tau s}=M_{zz}^{\tau s}=E_{\tau s}^{\rho}, M_{xy}^{\tau s}=M_{xz}^{\tau s}=M_{yx}^{\tau s}=M_{yz}^{\tau s}=M_{zx}^{\tau s}=M_{zy}^{\tau s}=0
\end{aligned}
\tag{23}
$$

The corresponding mechanical and natural boundary conditions can be also simplified as follows:

$$
\begin{aligned}
U_{xs}&=0\\
U_{ys_{,y}}&=0\\
U_{zs}&=0
\end{aligned}
\tag{24}
$$

Equation (22) is assessed for kth layer and can be assembled into a global algebraic eigensystem in the light of contribution of each layer. Layer-wise theory is used to fulfill this procedure, which can be referred to Pagani et al. [43] for the sake of simplicity. In this paper, LW models are implemented by utilizing one or more LE expansions on the cross-sectional domain of each layer, as discussed in the following sections. As a consequence, the theory kinematics can be opportunely varied at layer level by setting the order of LE expansions. This characteristic of LE CUF beam models allows the implementation of higher-order LW models in an easy and straightforward manner.

3 Numerical results

To demonstrate the exactness of the proposed quasi-3D model on the basis of CUF, free vibration analysis of simply supported composite beams with solid and thin-walled cross sections are investigated. The first part of this section focuses on the compact square cross-ply laminated beams considering different slenderness ratios, number of layers for laminates and material properties between layers, while the second part of this section presents thin-walled composite beams with complex geometries, i.e., hollow box and T-shaped cross sections.

3.1 Laminated beams

3.1.1 Two- and three-layer laminated beams

Square-sectional beams, consisting of two-layer [0/90] and three-layer [0/90/0] laminates of the same thickness, are considered in the first assessment. The dimensions of the beam are of equal width and height: $b = h = 0.2$m, being two kinds of slenderness ratios: $l/b = 100$ (slender beam) and $l/b = 5$ (short beam). The material is assumed to be orthotropic with the following properties: Young modulus: $E_L = 250$ GPa, $E_T = 10$ GPa; Poisson ratio: $\nu_{LT} = \nu_{TT} = 0.33$; Material density: $\rho = 2700$ kg/m^3; Shear modulus: $G_{LT} = 5$

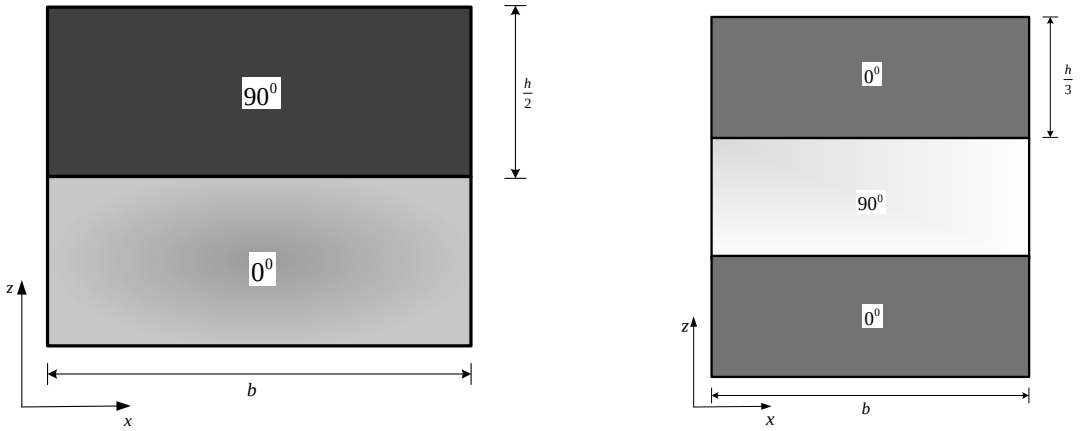

(a) The cross section for a two-layer composite beam.

(b) The cross section for a three-layer composite beam.

Figure 2: Cross sections for two- and three-layer laminated beams.

GPa, $G_{TT} = 2$ GPa, where the subscripts L and T represent the direction parallel and perpendicular to the fibres, respectively.

Unless differently specified, we use the notation $\zeta \times \eta \mathrm{L}\beta$ to denote beams of square cross sections, whereas $\vartheta \mathrm{L}\beta$ to denote those of thin-walled cross sections, where ζ and η stand for the number of Lβ elements in the x direction and z direction, ϑ stands for the number of Lβ elements over the whole cross section, and β stands for bilinear(4), cubic(9) and fourth-order(16) Lagrange polynomials, respectively.

Fig. 2(a) and Fig. 2(b) present the cross sections of the laminated beams addressed.

Tables 1 and 3 show a list of the first four non-dimensional natural frequencies with one half wave number ($m = 1$) for slender ($l/b = 100$) two- and three-layer composite beams. Moreover, in Tables 2 and 4 the first five non-dimensional natural frequencies with one half wave number ($m = 1$) for short ($l/b = 5$) two- and three-layer composite beams are given. The number of Degrees of Freedoms (DOFs) for different models are also reported in the second column of the tables. The results obtained by various LE models are compared with the classical beam models, including Euler-Bernoulli beam model (EBBM) and Timoshenko beam model (TBM), and refined closed-form CUF-TE solutions provided by Giunta et al. [35]. Three-dimensional finite element model created by Ansys software also serves as a benchmark for the same assessment, where the quadratic solid element SOLID 186 is used. Two different mesh schemes (coarse mesh and refined mesh) are adopted to ensure the convergence, and the notation FEM 3D$_n$ denotes the solid model with n elements along the x-axis, $n \times 10$ elements along y-axis, and n elements along z. The results are given in terms of the

Table 1: First four non-dimensional natural frequencies ω^* for a two-layer composite beam [0/90] with m=1, $L/b = 100$.

Model	DOFs	mode 1[a]	mode 2[b]	mode 3[c]	mode 4[d]
FEM $3D_8$[f][35]	74115	6.1690	10.254	176.99	1131.1
FEM $3D_6$[g][35]	33159	6.1690	10.254	177.00	1131.1
TBM [35]	10	6.1678	10.261	-[e]	1131.6
EBBM [35]	6	6.1712	10.272	-	1132.7
Refined CUF-TE Theory [35]					
$N = 2$	18	6.1726	10.268	201.60	1132.3
$N = 8$	135	6.1694	10.255	178.78	1131.3
$N = 15$	408	6.1691	10.254	177.84	1131.2
Present CUF-LE Theory					
1×2L4	18	6.1841	10.272	192.91	1131.8
2×2L4	27	6.1839	10.264	192.91	1131.8
1×2L9	45	6.1700	10.257	183.77	1131.2
2×2L9	75	6.1699	10.254	178.35	1131.2
1×2L16	84	6.1692	10.254	177.09	1131.2
2×2L16	147	6.1691	10.254	177.05	1131.1

[a]: Flexural mode on plane yz
[b]: Flexural (plane xy)/torsional mode
[c]: Torsional mode
[d]: Axial/shear (plane yz) mode
[e]: Mode not provided by the theory
[f]: The number of elements is $8 \times 80 \times 8$
[g]: The number of elements is $6 \times 60 \times 6$

following non-dimensional natural frequency ω^*:

$$\omega^* = (\omega L^2/b)\sqrt{\rho/E_{22}} \tag{25}$$

From Table 1, it can be seen that the present CUF-LE theory with even the simplest elements (1×2L4 and 2×2L4) shows the same accuracy as EBBM and TBM. On the other hand, the results obtained by the higher-order LW proposed models achieve faster convergence to the refined FEM $3D^g$ than refined CUF-TE theories [35].

In the case of short beams, EBBm is proved to be incapable of obtaining the correct result and so has TBM (but mode 1), which is shown in Table 2. In addition, present lower-order CUF-LE models (1×2L4 and 2×2L4) and refined lower-order CUF-TE model ($N = 2$) yield poor results in mode 4 and mode 5, i.e. in the case of axial and shear modes. Conversely, higher-order models making use of L9 and L16 LW approximation can produce the same results as 3D FEM solutions with less computational costs.

From Table 3 and 4, it is obvious that the majority of modes are symmetric modes without coupling effects except for mode 5 in the case of $l/b = 5$. Meanwhile, it is noteworthy that EBBM and TBM are considered not sufficient for predicting the first two modes in Table 4. Moreover, more attention should be paid to model 3×3L9 and 1×3L16, which produce approximately the same solutions independently from

Table 2: First five non-dimensional natural frequencies ω^* for a two-layer composite beam [0/90] with m=1, $L/b = 5$

Model	DOFs	mode 1[a]	mode 2[b]	mode 3[c]	mode 4[d]	mode 5[e]
FEM $3D_20$[g][35]	1037043	4.9357	6.4491	9.0672	33.566	50.448
FEM $3D_6$[h][35]	33159	4.9387	6.4520	9.0698	33.564	50.441
TBM [35]	10	5.0748	7.5056	-[f]	40.959	-
EBBM [35]	6	6.0098	10.104	-	57.194	-
Refined CUF-TE Theory [35]						
$N = 2$	18	5.0561	6.9642	10.134	37.566	63.563
$N = 10$	198	4.9413	6.4779	9.1134	33.910	50.923
$N = 15$	408	4.9388	6.4663	9.0958	33.803	50.749
$N = 23$	900	4.9375	6.4603	9.0852	33.718	50.640
Present CUF-LE theory						
1×2L4	18	5.0529	6.8718	9.7712	36.406	60.331
2×2L4	27	5.0528	6.8698	9.7710	36.406	60.305
1×2L9	45	5.0186	6.6664	9.4863	33.624	55.646
2×2L9	75	5.0185	6.4716	9.1681	33.623	51.560
1×2L16	84	4.9359	6.4518	9.0753	33.568	50.736
2×2L16	147	4.9358	6.4504	9.0708	33.568	50.564

[a]: Flexural mode on plane yz

[b]: Flexural (plane xy)/torsional mode

[c]: Torsional mode

[d]: Axial/shear (plane yz) mode

[e]: Shear mode on plane xz

[f]: Mode not provided by the theory

[g]: The number of elements is $20 \times 200 \times 20$

[h]: The number of elements is $6 \times 60 \times 6$

Table 3: First four non-dimensional natural frequencies ω^* for a three-layer composite beam [0/90/0] with m=1, $l/b = 100$

Model	DOFs	mode 1[a]	mode 2[b]	mode 3[c]	mode 4[d]
FEM $3D_9$[f][35]	103440	11.727	13.932	174.00	1295.4
FEM $3D_6$[g][35]	33159	11.727	13.932	174.01	1295.4
TBM [35]	10	11.730	13.955	-[e]	1295.4
EBBM [35]	6	11.747	13.989	-	1295.4
Refined CUF-TE Theory[35]					
$N = 2$	18	11.743	13.963	209.44	1296.6
$N = 8$	135	11.729	13.935	176.10	1295.5
$N = 15$	408	11.727	13.934	175.52	1295.4
$N = 23$	900	11.727	13.933	174.89	1295.4
Present CUF-LE Theory					
1×3L4	24	11.745	13.941	182.47	1295.9
3×3L4	48	11.734	13.938	179.70	1295.8
1×3L9	63	11.731	13.933	179.84	1295.5
3×3L9	147	11.727	13.933	174.39	1295.4
1×3L16	120	11.727	13.932	174.09	1295.4
3×3L16	300	11.727	13.932	174.01	1295.4

[a]: Flexural mode on plane xy

[b]: Flexural mode on plane yz

[c]: Torsional mode

[d]: Axial mode

[e]: Mode not provided by the theory

[f]: The number of elements is $9 \times 90 \times 9$

[g]: The number of elements is $6 \times 60 \times 6$

Table 4: First five non-dimensional natural frequencies ω^* for a three-layer composite beam [0/90/0] with m=1, $l/b = 5$

Model	DOFs	mode 1[a]	mode 2[b]	mode 3[c]	mode 4[d]	mode 5[e]
FEM $3D_24$[g][35]	1769475	6.8888	7.4965	9.0386	55.536	57.912
FEM $3D_12$[h][35]	235443	6.8894	7.4972	9.0391	55.536	57.913
TBM [35]	10	8.0411[b]	8.0850[a]	-[f]	-	64.766
EBBM [35]	6	11.553[b]	13.753[a]	-	-	64.766
Refined CUF-TE Theory[35]						
$N = 2$	18	8.0453[b]	8.0834[a]	10.502	62.746	67.230
$N = 10$	198	6.9630	7.5137	9.0957	56.639	58.411
$N = 15$	408	6.9420	7.5056	9.0907	56.091	58.284
$N = 23$	900	6.9252	7.5017	9.0683	55.914	58.135
Present CUF-LE Theory						
1×3L4	24	7.0118	7.9672	9.5019	62.525	66.253
3×3L4	48	7.0114	7.7949	9.3338	62.522	62.529
1×3L9	63	6.9047	7.8322	9.4216	57.926	61.386
3×3L9	147	6.9047	7.5044	9.0753	55.852	57.925
1×3L16	120	6.8889	7.4996	9.0479	55.845	57.917
3×3L16	300	6.8888	7.4968	9.0393	55.587	57.917

[a]: Flexural mode on plane yz
[b]: Flexural mode on plane xy
[c]: Torsional mode
[d]: Shear mode on plane xz
[e]: Axial/shear (plane yz) mode
[f]: Mode not provided by the theory
[g]: The number of elements is $24 \times 240 \times 24$
[h]: The number of elements is $12 \times 120 \times 12$

the number of DOFs. This important observation implies that CUF-LE model with higher order expansion is able to detect each mode exactly regardless of the slenderness ratio though lacking enough elements in both x and z directions.

Three selected mode shapes, i.e. mode 1, mode 2, and mode 4, concerning two- and three-layer composite beams ($l/b = 5$) and obtained by 2×2L16 and 3×3L16 models, are shown in Fig. 3. From these graphs, it should be underlined that coupled flexural/torsion and axial/shear phenomena appear when unsymmetric lamination is considered. Beyond that, shear mode on plane yz is apt to appear in mode 4 for the two-layer case, while mode 4 is dominated by shear mode on plane xz in the other case.

3.1.2 Nine- and Ten-layer laminated beams

This section aims to investigate the vibration characteristics of composite beam constructed by nine and ten layers. A ten-layer anti-symmetric and nine-layer symmetric cross-ply laminated beams are separately considered (see Fig. 4(a) and Fig. 4(b)). Tables 5 and 6 present the first five corresponding non-dimensional natural frequencies with $m = 1$ to $m = 5$ via the current model and 3D FEM software ABAQUS. From Table 5, it is possible to see that the present 5×10L16 model predicts lower values than 3D FEM model in most frequencies, which suggests that higher-order LE model with thousands of DOFs overcomes the results provided by 3D FEM model with one hundred thousands of DOFs. Again, 1×10L16 model can produce almost the same value in comparison with 5×10L9 with nearly half of its DOFs. Besides, as for higher number

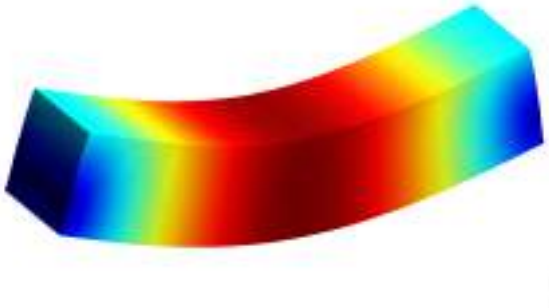

(a) Mode 1, Flexural mode on plane yz for a two-layer laminated beam ($L/b = 5$).

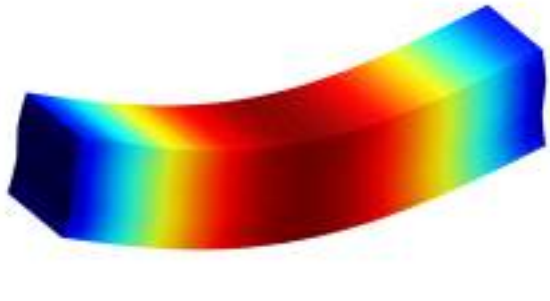

(b) Mode 1, Flexural mode on plane yz for a three-layer laminated beam ($L/b = 5$).

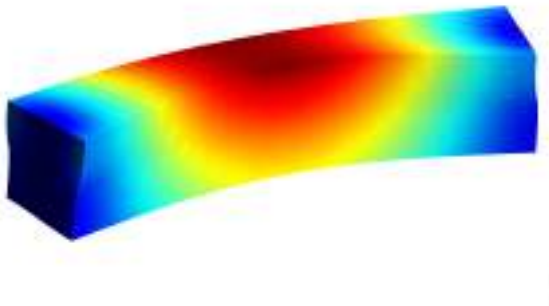

(c) Mode 2, Flexural (plane xy)/torsional mode for a two-layer laminated beam ($L/b = 5$)

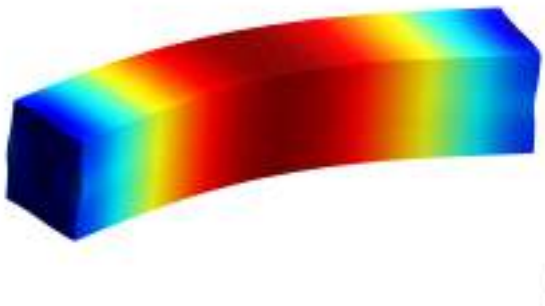

(d) Mode 2, Flexural mode on plane xy for a three-layer laminated beam ($L/b = 5$)

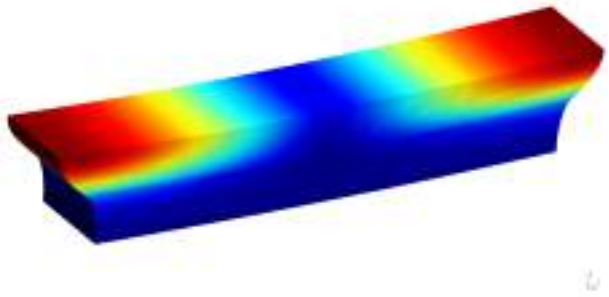

(e) Mode 4, Axial/shear (plane yz) mode for a two-layer laminated beam ($L/b = 5$)

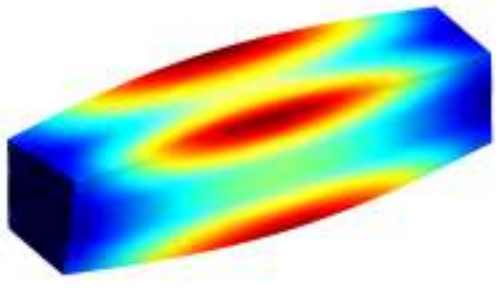

(f) Mode 4, Shear mode on plane xz for a three-layer laminated beam ($L/b = 5$)

Figure 3: Selected mode shapes of two- and three-layer laminated beams of Table 1 and Table 2 via the 2×2L16 and 3×3L16 model, m=1.

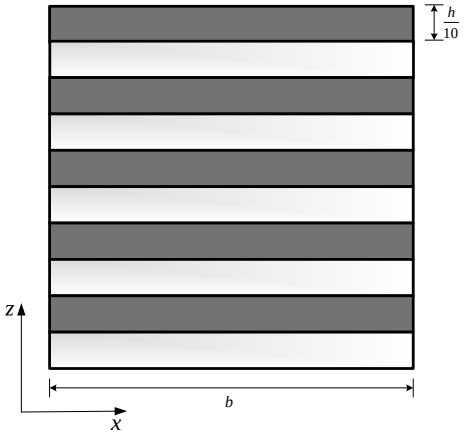

(a) The cross section for a ten-layer composite beam.

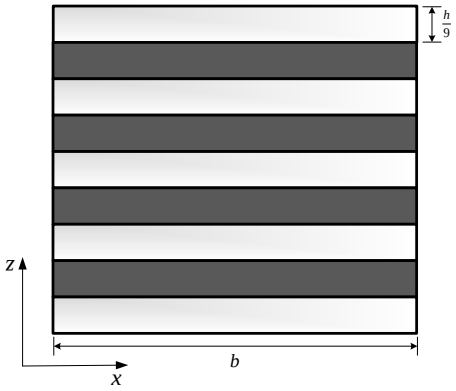

(b) The cross section for a nine-layer composite beam.

Figure 4: cross sections for nine- and ten-layer laminated beams.

of half-waves ($m = 2$ and $m = 4$) the lower-order model (2×10L4) interchanges the order of appearance for the following two cases (see mode 5 in $m = 2$ and mode 4 in $m = 4$). The same conclusion, i.e., the high efficiency in higher-order model and modal confusion in lower-order model, can be also observed in Table 6. Comparing Table 6 and Table 5, it is worth mentioning that each modes remain almost the same for both of cases, regardless of the value of m. Figures 5 and 6 display the lowest mode shapes 1-8 corresponding to anti-symmetric and symmetric cross-ply laminated composite beams ($l/b = 5$) via 5×10L16 model and 5×9L16 model, with $m = 1$ to 5. Out of these figures, it is important to underline that for higher m values ($m = 2$ and $m = 3$), torsion mode tends to appear before the dominant flexural mode on plane xy in both of cases.

3.2 Sandwich beam

A three-layer sandwich beam with a soft core is further considered (see Fig. 7). The geometric parameters of the beam are as follows: $b = h = 0.2$, length-to-width ratio $l/b = 5$. The thicknesses of top face and bottom face are equal: $h_f = h_b = 0.02$m, whereas the thickness of the core is $h_c = 0.16$m. The material properties are given in Table 7. The first five non-dimensional natural frequencies with m=1 to 5, computed by the present model and 3D FEM solutions, are reported in Table 8. From this table, it can be seen that as m increases, the gap between each mode (Modes 1-5) decreases, especially in the case $m = 5$, which signifies the difficulty to capture the corresponding natural frequencies with a desired level of accuracy. Moreover, Table 8 also provide ABAQUS models solutions for both reduced and full integration scheme in order to underline the numerical deficiencies in FE solutions. The core modes obtained via the 6×9L16 model, with $m = 1$ to 5, are shown in Fig. 8. Observing these mode shapes, we can see that core modes occur accompanied by the significant deformation of the soft core, which are characterised by symmetric and anti-symmetric mode shapes in sequential order.

Table 5: First five non-dimensional natural frequencies ω^* for a ten-layer anti-symmetric cross-ply laminated composite beam with m=1 to 5, $l/b = 5$

Cross section			Non-dimensional Natural Frequencies				
Seq.	Model	DOFs	Mode:1	2	3	4	5
	2×10L4	99	6.0691	7.4838	9.2709	55.520	58.574
	1×10L9	189	6.0520	7.4580	9.2416	55.151	58.274
$m = 1$	5×10L9	693	6.0518	7.1650	8.9023	53.697	55.148
	1×10L16	372	6.0517	7.1659	8.9042	53.821	55.149
	5×10L16	1488	6.0516	7.1642	8.9007	53.596	55.148
	FEM 3D[a]	111363	6.0517	7.1639	8.9007	53.675	55.146
	2×10L4		14.404	18.990	19.398	60.511	68.291
	1×10L9		14.347	18.920	19.285	60.187	67.406
$m = 2$	5×10L9		14.347	18.179	18.238	55.622	65.605
	1×10L16		14.345	18.202	18.256	55.754	65.784
	5×10L16		14.344	18.171	18.232	55.521	65.538
	FEM 3D[a]		14.346	18.172	18.232	55.598	65.522
	2×10L4		22.759	28.720	31.165	64.121	71.704
	1×10L9		22.662	28.603	30.958	63.756	70.845
$m = 3$	5×10L9		22.661	27.613	29.304	59.195	69.042
	1×10L16		22.648	27.667	29.409	59.353	69.246
	5×10L16		22.648	27.590	29.280	59.090	68.969
	FEM 3D[a]		22.658	27.594	29.275	59.162	68.951
	2×10L4		31.249	38.322	42.681	69.145	76.217
	1×10L9		31.116	38.162	42.385	68.730	75.382
$m = 4$	5×10L9		31.115	37.027	40.326	64.201	73.631
	1×10L16		31.073	37.113	40.559	64.415	73.869
	5×10L16		31.073	36.974	40.268	64.078	73.544
	FEM 3D[a]		31.109	36.991	39.743	64.147	73.527
	2×10L4		39.918	47.771	54.049	75.392	81.638
	1×10L9		39.755	47.568	53.672	74.926	80.817
$m = 5$	5×10L9		39.754	46.367	51.323	70.456	79.163
	1×10L16		39.655	46.449	51.695	70.753	79.418
	5×10L16		39.655	46.265	51.220	70.299	79.046
	FEM 3D[a]		39.743	46.313	51.196	70.363	79.039

[a]: The number of elements is $12 \times 67 \times 10$

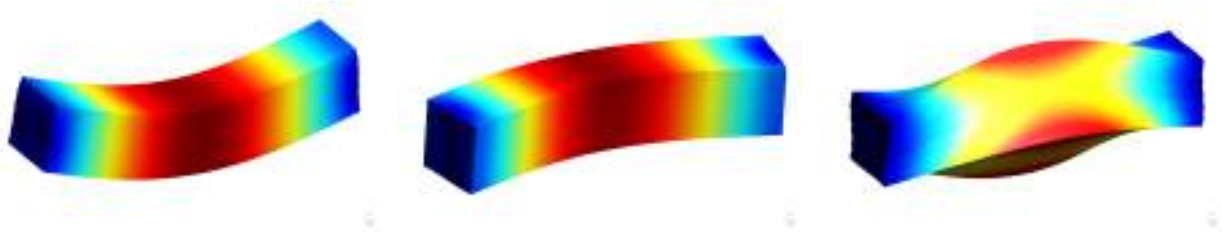

(a) $m = 1$, Flexural mode on plane yz ($\omega^* = 6.0516$)

(b) $m = 1$, Flexural (plane xy)/torsional mode ($\omega^* = 7.1642$)

(c) $m = 1$, Torsional mode ($\omega^* = 8.9007$)

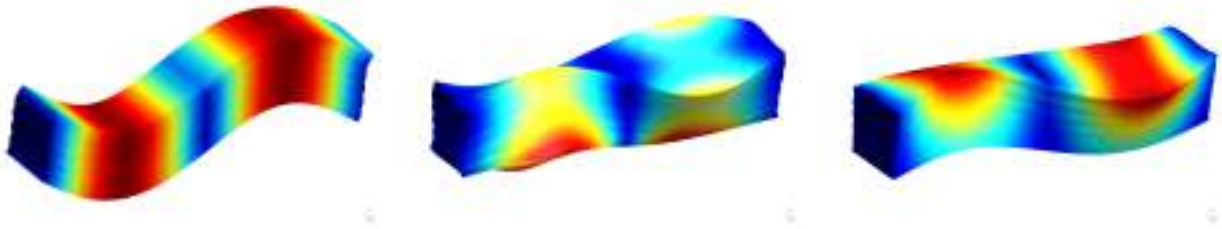

(d) $m = 2$, Flexural mode on plane yz ($\omega^* = 14.344$)

(e) $m = 2$, Torsional mode ($\omega^* = 18.171$)

(f) $m = 2$, Flexural (plane xy)/torsional mode ($\omega^* = 18.232$)

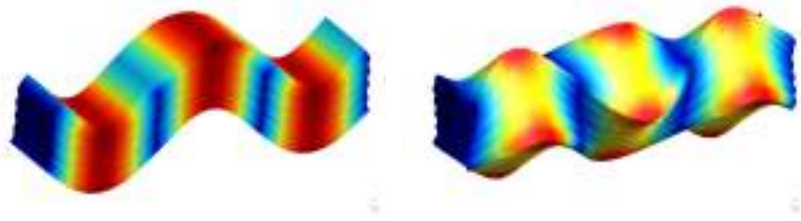

(g) $m = 3$, Flexural mode on plane yz ($\omega^* = 22.648$)

(h) $m = 3$, Torsional mode ($\omega^* = 27.590$)

Figure 5: The lowest mode shapes 1-8 for an anti-symmetric cross-ply ten-layer laminated composite beam ($l/b = 5$) of Table 5 via the 5×10L16 model, with m=1 to 3.

Table 6: First five non-dimensional natural frequencies ω^* for a nine-layer symmetric cross-ply laminated composite beam with m=1 to 5, $l/b = 5$

Cross section			Non-dimensional Natural Frequencies				
Seq.	Model	DOFs	Mode:1	2	3	4	5
	2×9L4	90	6.5898	7.6930	9.2583	58.791	58.937
	1×9L9	171	6.5692	7.6637	9.2318	58.407	58.484
$m = 1$	5×9L9	627	6.5690	7.3490	8.8962	53.721	58.482
	1×9L16	336	6.5688	7.3500	8.8988	53.861	58.482
	5×9L16	1344	6.5687	7.3482	8.8941	53.607	58.481
	FEM 3D[a]	171687	6.5688	7.3478	8.8944	53.684	58.480
	2×9L4		15.325	18.947	19.652	61.000	68.597
	1×9L9		15.259	18.885	19.531	60.594	67.476
$m = 2$	5×9L9		15.259	18.203	18.449	55.901	65.554
	1×9L16		15.255	18.227	18.477	56.052	65.741
	5×9L16		15.255	18.193	18.441	55.787	65.480
	FEM 3D[a]		15.258	18.195	18.440	55.862	65.453
	2×9L4		24.093	28.695	31.409	64.916	71.980
	1×9L9		23.982	28.591	31.188	64.476	70.907
$m = 3$	5×9L9		23.981	27.711	29.541	59.774	69.009
	1×9L16		23.961	27.778	29.661	59.959	69.231
	5×9L16		23.961	27.677	29.514	59.655	68.925
	FEM 3D[a]		23.977	27.687	29.508	59.727	68.899
	2×9L4		33.024	38.413	42.918	70.262	76.518
	1×9L9		32.875	38.268	42.603	69.781	75.496
$m = 4$	5×9L9		32.875	37.304	40.584	65.100	73.686
	1×9L16		32.811	37.401	40.840	65.349	73.946
	5×9L16		32.811	37.224	40.519	64.959	73.574
	FEM 3D[a]		32.865	37.257	40.503	65.030	73.557
	2×9L4		42.153	48.089	54.288	76.814	82.042
	1×9L9		41.977	47.911	53.884	76.294	81.067
$m = 5$	5×9L9		41.976,	46.93	51.609	71.654	79.396
	1×9L16		41.830	47.006	52.008	71.986	79.668
	5×9L16		41.830	46.774	51.492	71.470	79.229
	FEM 3D[a]		41.959	46.854	51.239	71.541	79.238

[a]: The number of elements is $20 \times 70 \times 9$

Table 7: Material properties for core and face

	Core	Face
E_1 (MPa)	0.2208	131100
E_2 (MPa)	0.2001	6900
E_3 (MPa)	2760	6900
G_{12} (MPa)	16.56	3588
G_{23} (MPa)	455.4	2332.2
G_{13} (MPa)	545.1	3088
ν_{12}	0.99	0.32
ν_{23}	0.00003	0.49
ν_{13}	0.00003	0.32
ρ (kg/m^3)	70	1000

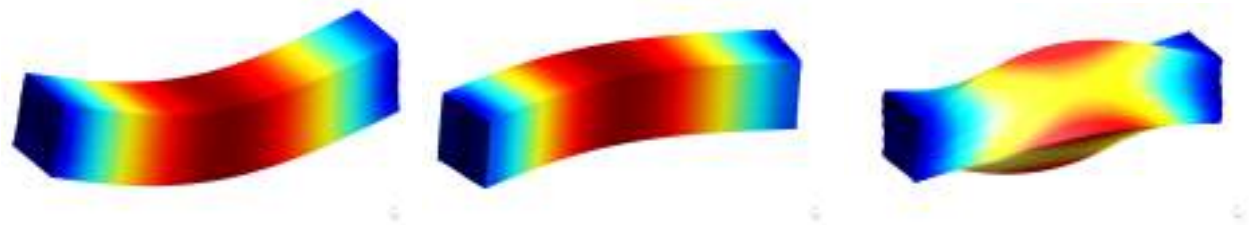

(a) $m = 1$, Flexural mode on plane yz ($\omega^* = 6.5687$) (b) $m = 1$, Flexural mode on plane xy ($\omega^* = 7.3482$) (c) $m = 1$, Torsional mode ($\omega^* = 8.8941$)

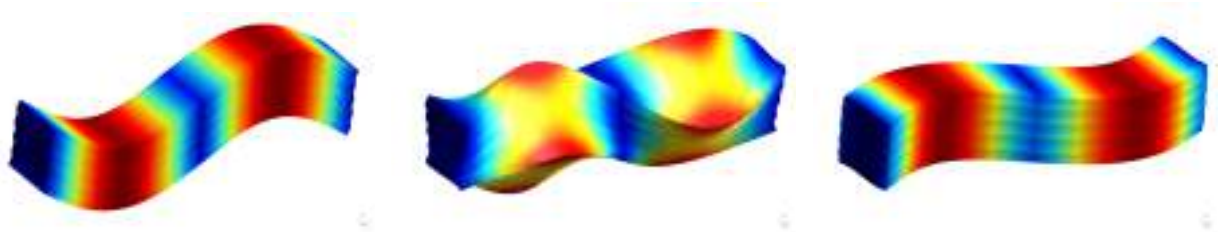

(d) $m = 2$, Flexural mode on plane yz ($\omega^* = 15.255$) (e) $m = 2$, Torsional mode ($\omega^* = 18.193$) (f) $m = 2$, FLEXURAL MODE ON PLANE xy C($\omega^* = 18.441$)

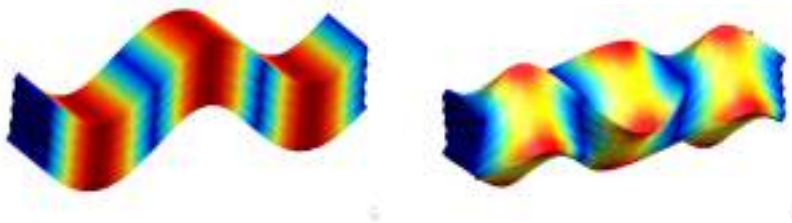

(g) $m = 3$, Flexural mode on plane yz (h) $m = 3$, Torsional mode ($\omega^* = 27.677$) ($\omega^* = 23.961$)

Figure 6: The lowest mode shapes 1-8 for a symmetric nine-layer cross-ply laminated composite beam ($l/b = 5$) of Table 6 via the 5×9L16 model, with m=1 to 3.

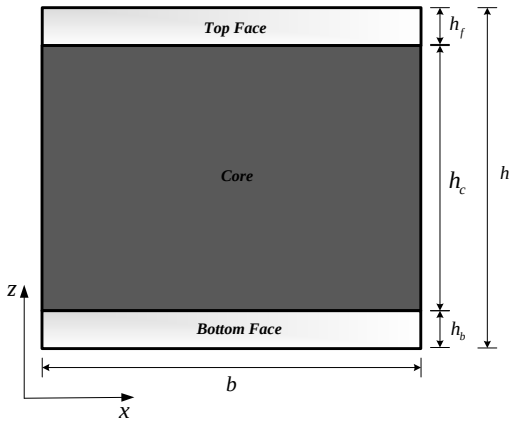

Figure 7: The cross section for a sandwich beam.

Table 8: First five non-dimensional natural frequencies ω^* for a three-layer sandwich beam [0/0/0] with m=1 to 5, $l/b = 5$

Cross section			Non-dimensional Natural Frequencies				
Seq.	Model	DOFs	Mode:1	2	3	4	5
	3×5L4	72	7.2431	7.8286	9.3783	50.110	57.653
	3×5L9	231	7.0761	7.8151	9.1907	47.292	48.708
$m = 1$	3×8L9	357	7.0761	7.8151	9.1907	47.290	48.631
	4×6L16	741	7.0693	7.8150	9.1812	44.590	46.013
	6×9L16	1596	7.0693	7.8150	9.1810	43.525	44.771
	FEM 3D[a]	70323	7.0692	7.8150	9.1814	43.177	44.347
	FEM 3D[b]	70323	7.0693	7.8150	9.1812	43.883	45.181
	3×5L4		17.296	17.816	19.716	52.428	60.154
	3×5L9		17.248	17.264	19.263	49.377	49.639
$m = 2$	3×8L9		17.248	17.264	19.263	49.298	49.637
	4×6L16		17.206	17.243	19.213	45.056	46.542
	6×9L16		17.205	17.243	19.212	43.931	45.233
	FEM 3D[a]		17.204	17.247	19.215	43.558	44.781
	FEM 3D[b]		17.205	17.244	19.213	44.308	45.663
	3×5L4		26.955	28.165	30.260	56.493	61.533
	3×5L9		26.848	27.281	29.617	50.558	52.613
$m = 3$	3×8L9		26.848	27.281	29.617	50.477	52.511
	4×6L16		26.821	27.090	29.481	45.846	47.469
	6×9L16		26.821	27.078	29.478	44.613	46.050
	FEM 3D[a]		26.847	27.075	29.489	44.194	45.550
	FEM 3D[b]		26.822	27.084	29.481	45.023	46.512
	3×5L4		37.037	38.180	40.909	62.104	63.464
	3×5L9		36.846	36.938	40.150	52.254	54.564
$m = 4$	3×8L9		36.846	36.935	40.150	52.167	54.460
	4×6L16		36.449	36.752	39.889	46.924	48.948
	6×9L16		36.373	36.751	39.879	45.531	47.411
	FEM 3D[a]		36.350	36.843	39.918	45.048	46.854
	FEM 3D[b]		36.403	36.757	39.888	45.989	47.902
	3×5L4		47.567	47.749	51.662	65.854	69.013
	3×5L9		45.822	47.268	50.826	54.396	57.372
$m = 5$	3×8L9		45.809	47.267	50.825	54.301	57.271
	4×6L16		44.283	47.038	48.221	50.409	51.788
	6×9L16		43.729	46.621	47.038	50.389	50.477
	FEM 3D[a]		43.508	47.263	46.051	50.486	50.010
	FEM 3D[b]		43.934	47.139	47.054	50.407	50.865

[a]: The number of elements is $10 \times 50 \times 10$ using reduced integration,

[b]: The number of elements is $10 \times 50 \times 10$ using full integration.

(a) $m = 1$, Core mode ($\omega^* = 43.525$)

(b) $m = 1$, Core mode ($\omega^* = 44.771$)

(c) $m = 2$, Core mode ($\omega^* = 43.931$)

(d) $m = 2$, Core mode ($\omega^* = 45.233$)

(e) $m = 3$, Core mode ($\omega^* = 44.613$)

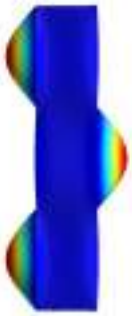

(f) $m = 3$, Core mode ($\omega^* = 46.050$)

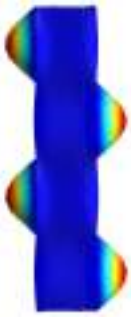

(g) $m = 4$, Core mode ($\omega^* = 47.411$)

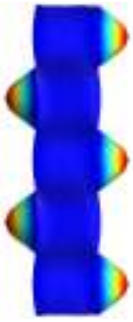

(h) $m = 5$, Core mode ($\omega^* = 50.477$)

Figure 8: The core modes from the top view for a three-layer sandwich beam of Table 8 via the 6×9L16 model, with m=1 to 5.

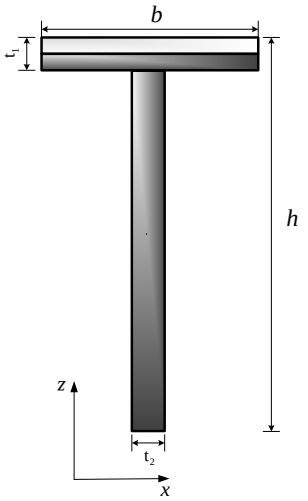

Figure 9: The cross section for a T-shaped composite beam.

3.3 T-shaped composite beam

After assessing the performance of the LE method in composite beams with rectangular cross sections, a T-shaped thin-walled composite beam is then considered (see Fig. 9). The structure has the following geometric characteristics: width $b = 0.1$m, height $h = 0.2$m, slenderness ratio $l/b = 10$, thickness of flange $t_1 = 0.01$m, thickness of web $t_2 = 0.01$m. The flange is composed of two cross-ply laminations [0/90] of the same thickness, while the web is made up of one lamination [0]. The material properties are: $E_L = 144$ MPa, $E_T = 9.65$ MPa, $G_{LT} = 4.14$ MPa, $G_{TT} = 3.45$ MPa, $\nu_{LT} = \nu_{LT}$=0.3, $\rho = 1389$ kg/m^3. Table 9 shows the first five natural frequencies with m=1-5 by the LE model and 3D FEM model. As may be noted from Table 9, the lower-order LE model (L4) provides good results with enough DOFs and the higher-order LE models (L9 or L16) produce more accurate results than 3D FEM model. The lowest mode shapes corresponding to 1-9 via the 29L16 model, with m=1 to 4 are displayed in Fig. 10. As shown in Fig. 10, mode 1 is always featured by flexural mode on plane xy, whatever the value of m. Mode 2 for m=1 is torsion mode, being shell-like mode for other values of m. The flexural mode on plane yz tends to appear after the aforementioned three modes.

3.4 Single-bay composite box beam

In this section, further study is performed for the case of a single-bay composite box beam. The configuration of the cross section can be seen in Fig. 11. The dimensions of the cross section are $b = 0.1$m and $h = 0.2$m. The length to width ratio is $l/b = 10$. The thickness of the wall is $t = 0.01$. As in the previous analysis case, two layers [0/90] are included in the top and bottom flange, respectively. One layer [0] is employed for two

Table 9: First five natural frequencies (Hz) for a T-shaped composite beam with m=1 to 5, $l/b = 10$

Cross section			Non-dimensional Natural Frequencies				
Seq.	Model	DOFs	Mode:1	2	3	4	5
	43L4	234	68.889	260.89	536.75	537.82	1191.2
$m = 1$	29L9	483	68.508	258.56	466.50	535.88	1021.5
	29L16	984	68.362	258.45	465.26	535.74	1010.4
	FEM 3D[a]	126765	68.379	258.45	465.52	535.78	1013.0
	32L4		209.80	577.54	909.93	1233.0	1263.7
$m = 2$	29L9		208.69	519.96	889.74	1109.6	1227.8
	29L16		208.29	518.38	886.06	1100.7	1226.6
	FEM 3D[a]		208.31	518.57	887.06	1102.5	1226.9
	32L4		436.35	747.78	1293.7	1696.2	1848.7
$m = 3$	29L9		434.12	695.74	1160.3	1648.0	1830.2
	29L16		432.90	692.96	1147.3	1643.4	1825.5
	FEM 3D[a]		432.98	693.18	1149.2	1643.7	1826.7
	32L4		747.05	987.48	1474.1	2323.8	2335.9
$m = 4$	29L9		743.17	942.02	1345.0	2178.2	2290.1
	29L16		739.90	937.01	1330.4	2157.5	2278.3
	FEM 3D[a]		740.12	937.50	1332.5	2159.8	2281.4
	32L4		1134.4	1288.8	1721.5	2682.3	2747.6
$m = 5$	29L9		1126.8	1244.7	1609.8	2507.8	2605.5
	29L16		1119.5	1235.7	1592.6	2476.9	2586.2
	FEM 3D[a]		1120.1	1236.8	1594.7	2480.2	2591.4

[a]: The number of elements in each flange is $25 \times 50 \times 2$,
The number of elements in each web is $2 \times 50 \times 50$.

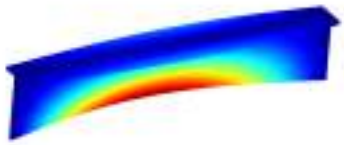

(a) $m = 1$, Flexural mode on plane xy ($f = 68.362$)

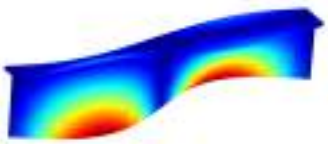

(b) $m = 2$, Flexural mode on plane xy ($f = 208.29$)

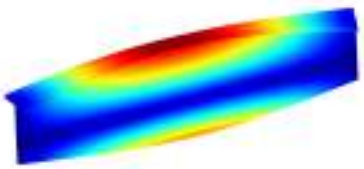

(c) $m = 1$, Torsional mode ($f = 258.45$)

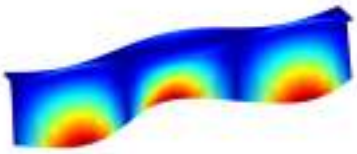

(d) $m = 3$, Flexural mode on plane xy ($f = 432.90$)

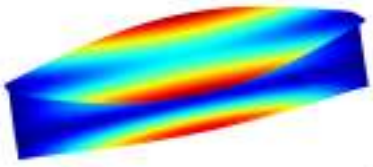

(e) $m = 1$, Shell-like mode ($f = 465.26$)

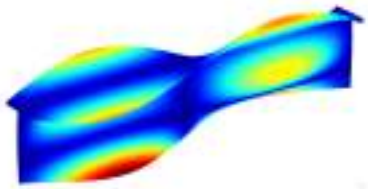

(f) $m = 2$, Shell-like mode ($f = 518.38$)

(g) $m = 1$, Flexural mode on plane yz ($f = 535.74$)

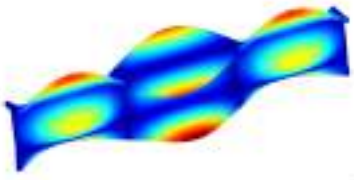

(h) $m = 3$, Shell-like mode ($f = 692.96$)

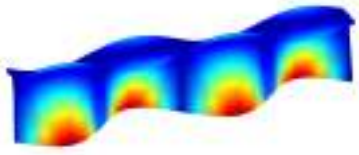

(i) $m = 4$, Flexural mode on plane xy ($f = 739.90$)

Figure 10: The lowest mode shapes 1-9 for a T-shaped laminated composite beam of Table 9 via the 29L16 model, with m=1 to 4.

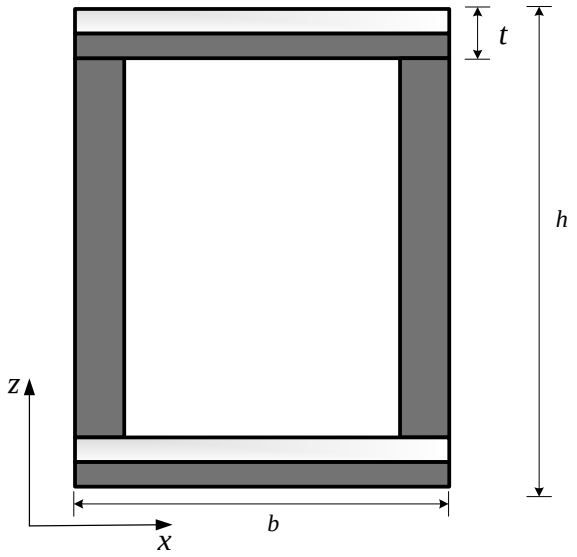

Figure 11: The cross section for a single-bay composite box beam.

webs. An orthotropic material is adopted for each layer in conformity to the case of T-shaped cross section. Table 10 shows the first five non-dimensional natural frequencies with m=1 to 5 acquired by the present model and 3D FEM model. Compared with the L4 results in the case of T-shaped and box beams, the proposed model is proved with poor capability to capture the warping phenomena. Thus, a higher-order model with enough DOFs is imperative in this case. In the end, comparison of the fifth mode shapes for m = 2 to 5, by 32L16 and 3D FEM model are shown in Fig. 12, providing satisfactory results.

3.5 Composite sandwich-box beam

The final example wants to demonstrate the enhanced and unique capability of the proposed LW beam model to address 3D problems. The cross section of the composite structure considered is thus shown in Fig. 13. The same geometrical shape of the cross section as for previous case is account for again, including a two-layer [0/90] laminate in the top and bottom faces, respectively, one layer [0] in the left and right faces, respectively, and a soft core is added in the middle. Also, the same material properties of the face and core are adopted as considered in the case of three-layer composite beam. Results are reported in Table 11. Although this structure is more complicated than the single-bay composite box beam, all modes under consideration are capable of being detected precisely via present 50L9 and 48L16 models. In particular, the comparison between 48L16 and 3D FEM model in forecasting the fifth mode shapes for m=2-5 is presented in Fig. 14. It is obvious that 48L16 model can describe the bending and core deformation phenomena correctly.

Table 10: First five natural frequencies (Hz) for a single-bay composite box beam with m=1 to 5, $l/b = 10$

Cross section			Non-dimensional Natural Frequencies				
Seq.	Model	DOFs	Mode:1	2	3	4	5
	32L4	168	341.19	553.77	605.07	1025.1	1080.4
	26L9	420	330.07	475.95	550.30	690.87	851.48
$m = 1$	32L9	528	325.64	469.70	549.94	635.73	847.12
	32L16	1062	323.89	466.62	549.67	622.59	844.16
	FEM 3D[a]	117789	323.50	466.22	549.59	622.03	843.62
	32L4		758.93	1109.3	1116.8	1287.0	1684.4
	26L9		659.97	734.00	956.48	1255.9	1470.8
$m = 2$	32L9		624.49	682.08	942.85	1253.1	1399.8
	32L16		614.04	669.53	939.17	1251.2	1383.8
	FEM 3D[a]		613.02	668.98	938.36	1251.1	1382.0
	32L4		1079.3	1190.7	1687.9	1973.4	2442.3
	26L9		849.22	873.41	1499.0	1786.6	2000.6
$m = 3$	32L9		804.62	819.94	1444.1	1721.4	1956.0
	32L16		793.12	805.19	1430.0	1700.0	1943.2
	FEM 3D[a]		792.64	804.07	1427.9	1699.6	1939.9
	32L4		1354.7	1356.8	2270.6	2585.9	3025.6
	26L9		1065.9	1114.3	2005.7	2046.2	2601.8
$m = 4$	32L9		1031.0	1062.8	1867.2	1921.9	2559.4
	32L16		1019.8	1047.1	1834.0	1891.2	2540.0
	FEM 3D[a]		1019.4	1046.2	1830.2	1890.2	2533.8
	32L4		1626.3	1667.9	2834.2	3065.6	3668.4
	26L9		1388.0	1440.2	2266.6	2460.8	3029.8
$m = 5$	32L9		1362.3	1396.6	2152.2	2238.4	2963.0
	32L16		1349.1	1378.9	2121.4	2189.5	2919.5
	FEM 3D[a]		1349.0	1378.1	2120.8	2184.9	2920.7

[a]: The number of elements in each flange is $15 \times 50 \times 2$,
The number of elements in each web is $3 \times 50 \times 15$.

Table 11: First five natural frequencies (Hz) for a composite sandwich-box beam with m=1 to 5, $l/b = 10$

Cross section			Non-dimensional Natural Frequencies				
Seq.	Model	DOFs	Mode:1	2	3	4	5
	5×10L4	198	353.83	607.31	673.49	1863.8	2702.5
	5×7L9	495	347.13	605.13	669.03	1353.4	1839.8
$m = 1$	5×10L9	693	346.40	604.87	668.22	1314.6	1785.7
	6×8L16	1425	345.25	604.69	666.98	1237.4	1673.6
	FEM 3D[a]	151008	345.10	604.68	666.65	1238.0	1674.4
	5×10L4		835.91	1389.8	1465.2	1892.9	2822.3
	5×7L9		791.92	1368.6	1385.6	1461.5	2003.2
$m = 2$	5×10L9		785.82	1347.5	1363.5	1460.2	1953.7
	6×8L16		775.95	1270.6	1354.9	1459.8	1849.0
	FEM 3D[a]		775.79	1271.1	1353.3	1459.7	1848.7
	5×10L4		1287.6	1964.9	2109.5	2310.4	3061.6
	5×7L9		1159.2	1472.5	2048.0	2305.5	2342.8
$m = 3$	5×10L9		1143.7	1436.0	2028.2	2300.4	2303.5
	6×8L16		1115.7	1361.2	1992.1	2212.0	2303.0
	FEM 3D[a]		1115.9	1361.7	1986.6	2209.7	2302.8
	5×10L4		1696.1	2107.7	2816.4	3142.5	3423.2
	5×7L9		1479.9	1646.6	2670.0	2822.2	3136.1
$m = 4$	5×10L9		1458.6	1613.5	2613.5	2783.7	3133.4
	6×8L16		1416.9	1543.5	2509.1	2706.5	2996.7
	FEM 3D[a]		1417.3	1543.9	2494.8	2701.3	2957.9
	5×10L4		2097.0	2344.7	3500.3	3872.5	3964.5
	5×7L9		1835.6	1930.4	3210.4	3360.1	3914.6
$m = 5$	5×10L9		1813.5	1901.7	3095.6	3322.3	3567.4
	6×8L16		1766.1	1837.1	2909.8	3188.4	3247.1
	FEM 3D[a]		1766.8	1837.8	2887.6	3151.4	3238.5

[a]: The number of elements is $15 \times 50 \times 15$,

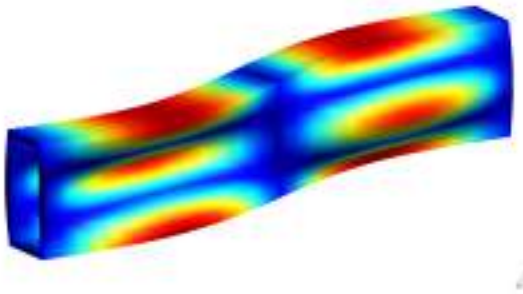

(a) 32L16, $m = 2$, Shell-like mode in the web ($f = 1383.8$)

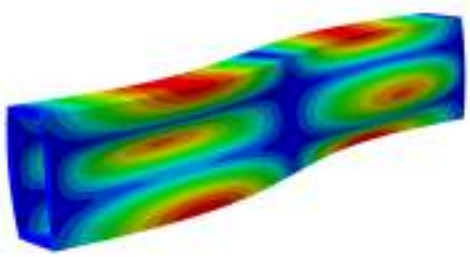

(b) ABAQUS, $m = 2$, Shell-like mode in the web ($f = 1382.0$)

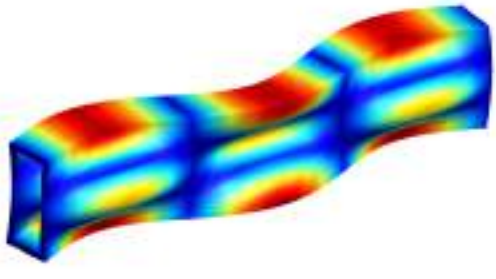

(c) 32L16, $m = 3$, Shell-like mode in the web ($f = 1943.2$)

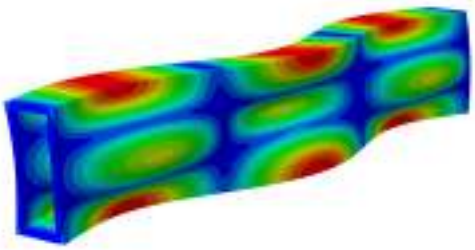

(d) ABAQUS, $m = 3$, Shell-like mode in the web ($f = 1939.9$)

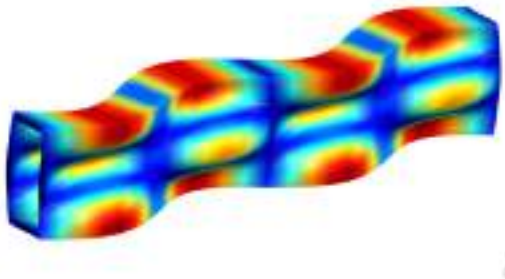

(e) 32L16, $m = 4$, Shell-like mode in the web ($f = 2540.0$)

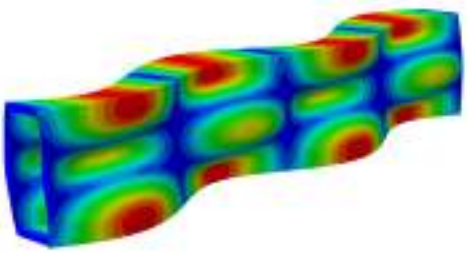

(f) ABAQUS, $m = 4$, Shell-like mode in the web ($f = 2533.8$)

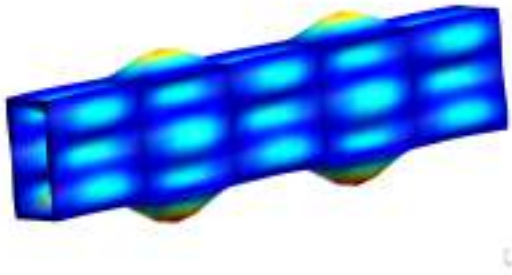

(g) 32L16, $m = 5$, Shell-like mode in the web ($f = 2919.5$)

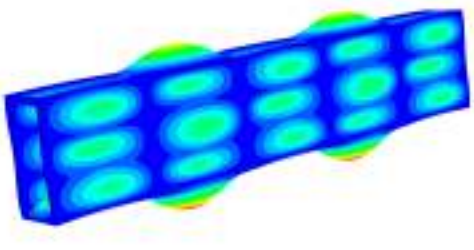

(h) ABAQUS, $m = 5$, Shell-like mode in the web ($f = 2920.7$)

Figure 12: Comparison of the fifth mode shapes for m=2-5, by 32L16 and 3D FEM model.

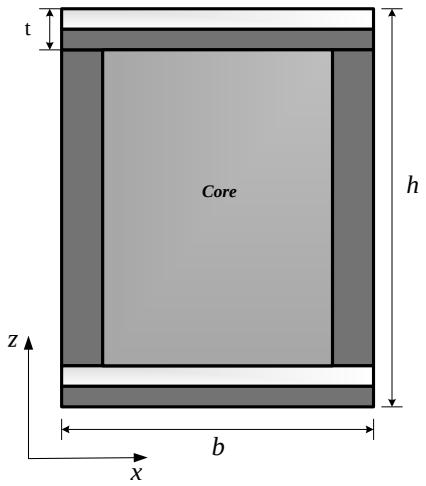

Figure 13: The cross section for a composite sandwich beam

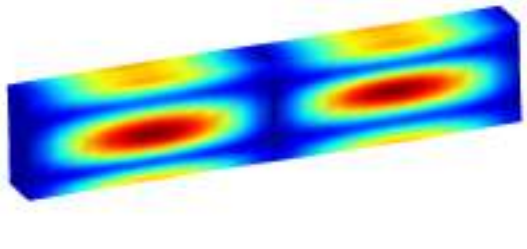

(a) 48L16, $m = 2$, Core mode ($f = 1849.0$)

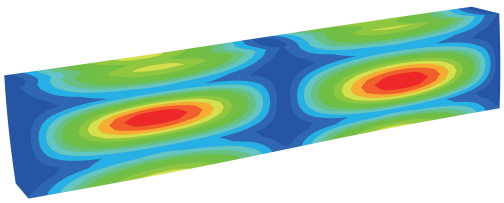

(b) ABAQUS, $m = 2$, Core mode ($f = 1848.7$)

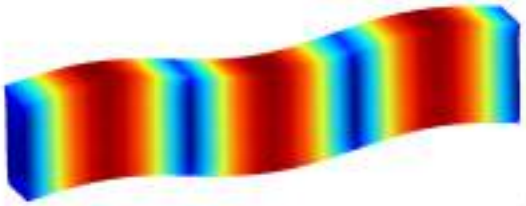

(c) 48L16, $m = 3$, Flexural mode on plane yz ($f = 2303.0$)

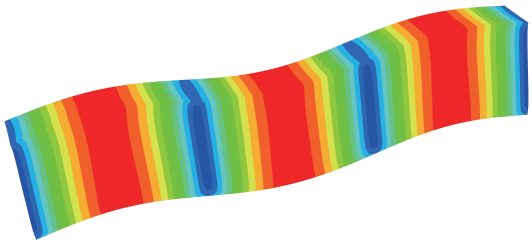

(d) ABAQUS, $m = 3$, Flexural mode on plane yz ($f = 2302.8$)

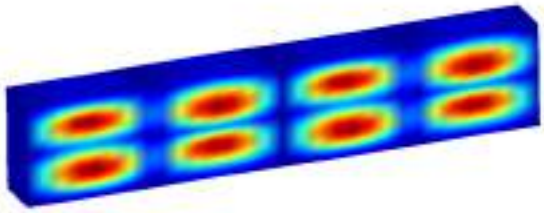

(e) 48L16, $m = 4$, Core mode ($f = 2996.7$)

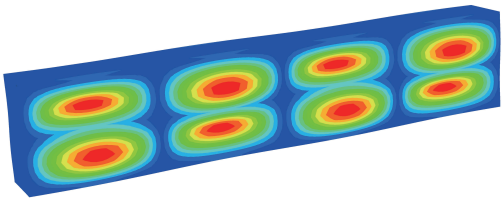

(f) ABAQUS, $m = 4$, Core mode ($f = 2957.9$)

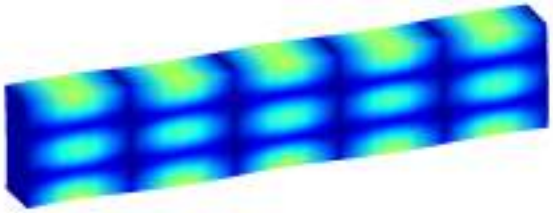

(g) 48L16, $m = 5$, Core mode ($f = 3247.1$)

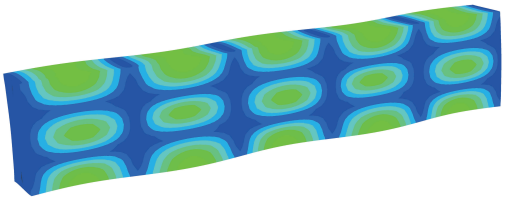

(h) ABAQUS, $m = 5$, Core mode ($f = 3238.5$)

Figure 14: Comparison of the fifth modes shape for m=2-5, by 48L16 and 3D FEM model.

4 Conclusions

In this paper, a unified closed-form formulation of refined beam models has been extended to the free vibration of simply supported cross-ply composite beams. The analysis has been performed in the domain of Carrera Unified Formulation, where 3D kinematic fields can be discretized as the expansion of any order of the cross-sectional node displacement unknowns via Lagrange Expansion (LE), being the ability of layer-wise naturally satisfied. The strong-form governing equation, derived by the principle of virtual displacement, can be solved by a Navier-type closed-form solution through the assumption of simply supported boundary conditions. Several numerical cases have been carried out to demonstrate the accuracy and effectiveness of the proposed methodology in comparison with 3D FEM results obtained from commercial code, including long and short cross-ply laminate beams with different stacking sequences, thin-walled composite beams and composite sandwich beams. From these results, the following conclusions can be drawn:

1. LE CUF model are considered to yield similar results as 3D FEM results, and more accurately than TE CUF model. This conclusion is more evident in the case of short compact beams.

2. Non-classical modes such as torsion, shear and axial/shear coupling modes can be detected with higher-order CUF LE model. Moreover, order of mode appearance may be interchanged each other for higher half wave numbers as the number of layer increases, which can be also captured by higher-order CUF LE model precisely.

3. In the case of heterogeneous structures with different material properties (e.g., sandwich beams) and when several natural frequencies fall in a narrow frequency spectrum, the use of lower/order beam models is not recommended.

4. Lower-order CUF LE model gives unsatisfactory mode results in the case of thin-walled composite beams (e.g., T-shaped and single-bay box shape). Meanwhile, higher-order CUF LE model with enough DOFs is capable of capturing the shell-like modes.

5. Concerning the beams with complex material properties (e.g., composite sandwich beams), the present model readily shows its high-efficiency over 3D FEM solutions.

Acknowledgments

The first author acknowledges the support by the scholarship from the China Scholarship Council (CSC) (Grant No. 201606710014) and Fundamental Research Funds for the Central Universities (Grant No. 2014B31414).

References

[1] Y. Yan, Q. W. Ren, N. Xia, and L. F. Zhang. A close-form solution applied to the free vibration of the euler–bernoulli beam with edge cracks. *Archive of Applied Mechanics*, 86(9):1633–1646, 2016.

[2] W. A. Oldfather, C. A. Ellis, and D. M. Brown. Leonhard euler's elastic curves. *Isis*, 20(1):72–160, 1933.

[3] E. Reissner. The effect of transverse shear deformation on the bending of elastic plates. *Journal of Applied Mechanics*, 12:69–77, 1945.

[4] R. D. Mindlin. Influence of rotary inertia and shear on flexural motions of isotropic elastic plates. *Journal of Applied Mechanics*, 18:31–38, 1951.

[5] K. Chandrashekhara, K. Krishnamurthy, and S. Roy. Free vibration of composite beams including rotary inertia and shear deformation. *Composite Structures*, 14(4):269–279, 1990.

[6] W. J. Chen, L. Li, and M. Xu. A modified couple stress model for bending analysis of composite laminated beams with first order shear deformation. *Composite Structures*, 93(11):2723–2732, 2011.

[7] A. A. Khdeir and J. N. Reddy. Free vibration of cross-ply laminated beams with arbitrary boundary conditions. *International Journal of Engineering Science*, 32(12):1971–1980, 1994.

[8] H. Arya, R. P. Shimpi, and N. K. Naik. A zigzag model for laminated composite beams. *Composite Structures*, 56(1):21–24, 2002.

[9] J. Li and H. X. Hua. Dynamic stiffness analysis of laminated composite beams using trigonometric shear deformation theory. *Composite Structures*, 89(3):433–442, 2009.

[10] P. Vidal and O. Polit. A family of sinus finite elements for the analysis of rectangular laminated beams. *Composite Structures*, 84(1):56–72, 2008.

[11] M. Karama, K. S. Afaq, and S. Mistou. Mechanical behaviour of laminated composite beam by the new multi-layered laminated composite structures model with transverse shear stress continuity. *International Journal of Solids and Structures*, 40(6):1525–1546, 2003.

[12] M. Karama, M. Touratier, and A. Idlbi. An evaluation of the edge solution for a higher-order laminated plate theory. *Composite Structures*, 25(1-4):495–502, 1993.

[13] F. G. Canales and J. L. Mantari. Buckling and free vibration of laminated beams with arbitrary boundary conditions using a refined hsdt. *Composites Part B: Engineering*, 100:136–145, 2016.

[14] R. P. Shimpi and A. V. Ainapure. Free vibration analysis of two layered cross-ply laminated beams using layer-wise trigonometric shear deformation theory. *Journal of Reinforced Plastics and Composites*, 21(16):1477–1492, 2002.

[15] M. Tahani. Analysis of laminated composite beams using layerwise displacement theories. *Composite Structures*, 79(4):535–547, 2007.

[16] T. S. Plagianakos and D. A. Saravanos. High-order layerwise mechanics and finite element for the damped dynamic characteristics of sandwich composite beams. *International Journal of Solids and Structures*, 41(24):6853–6871, 2004.

[17] E. Carrera. Historical review of zig-zag theories for multilayered plates and shells. *Applied Mechanics Reviews*, 56(3):287–308, 2003.

[18] H. Murakami. Laminated composite plate theory with improved in-plane responses. *Journal of Applied Mechanics*, 53(3):661–666, 1986.

[19] E. Carrera, M. Filippi, and E. Zappino. Laminated beam analysis by polynomial, trigonometric, exponential and zig-zag theories. *European Journal of Mechanics-A/Solids*, 41:58–69, 2013.

[20] M. Filippi and E. Carrera. Bending and vibrations analyses of laminated beams by using a zig-zag-layerwise theory. *Composites Part B: Engineering*, 98:269–280, 2016.

[21] A. Chakrabarti, H. D. Chalak, M. A. Iqbal, and A. H. Sheikh. A new fe model based on higher order zigzag theory for the analysis of laminated sandwich beam with soft core. *Composite Structures*, 93(2):271–279, 2011.

[22] M. K. Pandit, A. H. Sheikh, and B. N. Singh. An improved higher order zigzag theory for the static analysis of laminated sandwich plate with soft core. *Finite Elements in Analysis and Design*, 44(9):602–610, 2008.

[23] E. Carrera. Developments, ideas, and evaluations based upon reissners mixed variational theorem in the modeling of multilayered plates and shells. *Applied Mechanics Reviews*, 54(4):301–329, 2001.

[24] E. Carrera. Theories and finite elements for multilayered, anisotropic, composite plates and shells. *Archives of Computational Methods in Engineering*, 9(2):87–140, 2002.

[25] E. Carrera. Theories and finite elements for multilayered plates and shells: a unified compact formulation with numerical assessment and benchmarking. *Archives of Computational Methods in Engineering*, 10(3):215–296, 2003.

[26] E. Carrera and S. Brischetto. Analysis of thickness locking in classical, refined and mixed theories for layered shells. *Composite Structures*, 85(1):83–90, 2008.

[27] E. Carrera, G. Giunta, and M. Petrolo. *Beam structures: classical and advanced theories*. John Wiley & Sons, 2011.

[28] E. Carrera and M. Petrolo. On the effectiveness of higher-order terms in refined beam theories. *Journal of Applied Mechanics*, 78(2):021013, 2011.

[29] E. Carrera, G. Giunta, P. Nali, and M. Petrolo. Refined beam elements with arbitrary cross-section geometries. *Computers and structures*, 88(5):283–293, 2010.

[30] M. Petrolo, E. Zappino, and E. Carrera. Refined free vibration analysis of one-dimensional structures with compact and bridge-like cross-sections. *Thin-Walled Structures*, 56:49–61, 2012.

[31] A. Pagani, M. Boscolo, J. R. Banerjee, and E. Carrera. Exact dynamic stiffness elements based on one-dimensional higher-order theories for free vibration analysis of solid and thin-walled structures. *Journal of Sound and Vibration*, 332(23):6104–6127, 2013.

[32] A. Pagani, E. Carrera, and A. J. M. Ferreira. Higher-order theories and radial basis functions applied to free vibration analysis of thin-walled beams. *Mechanics of Advanced Materials and Structures*, 23(9):1080–1091, 2016.

[33] E. Carrera, A. Pagani, and J. R. Banerjee. Linearized buckling analysis of isotropic and composite beam-columns by carrera unified formulation and dynamic stiffness method. *Mechanics of Advanced Materials and Structures*, 23(9):1092–1103, 2016.

[34] E. Carrera, M. Filippi, and E. Zappino. Free vibration analysis of rotating composite blades via carrera unified formulation. *Composite Structures*, 106:317–325, 2013.

[35] G. Giunta, F. Biscani, S. Belouettar, A. J. M. Ferreira, and E. Carrera. Free vibration analysis of composite beams via refined theories. *Composites Part B: Engineering*, 44(1):540–552, 2013.

[36] A. Pagani, E. Carrera, M. Boscolo, and J. R. Banerjee. Refined dynamic stiffness elements applied to free vibration analysis of generally laminated composite beams with arbitrary boundary conditions. *Composite Structures*, 110:305–316, 2014.

[37] G. Giunta, D. Crisafulli, S. Belouettar, and E. Carrera. Hierarchical theories for the free vibration analysis of functionally graded beams. *Composite Structures*, 94(1):68–74, 2011.

[38] F. Fazzolari. Quasi-3d beam models for the computation of eigenfrequencies of functionally graded beams with arbitrary boundary conditions. *Composite Structures*, 154:239–255, 2016.

[39] E. Carrera and M. Petrolo. Refined beam elements with only displacement variables and plate/shell capabilities. *Meccanica*, 47(3):537–556, 2012.

[40] E. Carrera, M. Filippi, P. K. R. Mahato, and A. Pagani. Accurate static response of single-and multi-cell laminated box beams. *Composite Structures*, 136:372–383, 2016.

[41] E. Carrera, M. Filippi, P. K. R. Mahato, and A. Pagani. Advanced models for free vibration analysis of laminated beams with compact and thin-walled open/closed sections. *Journal of Composite Materials*, 49(17):2085–2101, 2015.

[42] M. Filippi, A. Pagani, M. Petrolo, G. Colonna, and E. Carrera. Static and free vibration analysis of laminated beams by refined theory based on chebyshev polynomials. *Composite Structures*, 132:1248–1259, 2015.

[43] A. Pagani, A. G. De Miguel, M. Petrolo, and E. Carrera. Analysis of laminated beams via unified formulation and Legendre polynomial expansions. *Composite Structures*, 156:78–92, 2016.

[44] G. Giunta, N. Metla, Y. Koutsawa, and S. Belouettar. Free vibration and stability analysis of three-dimensional sandwich beams via hierarchical models. *Composites Part B: Engineering*, 47:326–338, 2013.

[45] G. Giunta, S. Belouettar, H. Nasser, E. H. Kiefer-Kamal, and T. Thielen. Hierarchical models for the static analysis of three-dimensional sandwich beam structures. *Composite Structures*, 133:1284–1301, 2015.

[46] M. Dan, A. Pagani, and E. Carrera. Free vibration analysis of simply supported beams with solid and thin-walled cross-sections using higher-order theories based on displacement variables. *Thin-Walled Structures*, 98:478–495, 2016.

[47] J. N. Reddy. *Mechanics of laminated composite plates and shells: theory and analysis*. CRC press, 2004.

[48] E. Carrera, M. Cinefra, M. Petrolo, and E. Zappino. *Finite element analysis of structures through unified formulation*. John Wiley & Sons, 2014.